arXiv:1605.05919v2 [astro-ph.EP] 4 Oct 2016

Interpreting the librations of a synchronous satellite – How their phase assesses Mimas' global ocean

Benoît Noyelles

NAmur Center for CompleX SYStems (NAXYS) – University of Namur – Rempart de la Vierge 8 – B-5000 Namur – Belgium

benoit.noyelles@unamur.be

Received _____; accepted _____

ABSTRACT

Most of the main planetary satellites of our Solar System are expected to be in synchronous rotation, the departures from the strict synchronicity being a signature of the interior. Librations have been measured for the Moon, Phobos, and some satellites of Saturn. I here revisit the theory of the longitudinal librations in considering that part of the interior is not hydrostatic, i.e. has not been shaped by the rotational and tidal deformations, but is fossil. This consideration affects the rotational behavior.

For that, I derive the tensor of inertia of the satellite in splitting these two parts, before proposing an analytical solution that I validate with numerical simulations. I apply this new theory on Mimas and Epimetheus, for which librations have been measured from Cassini data.

I show that the large measured libration amplitude of these bodies can be explained by an excess of triaxiality that would not result from the hydrostatic theory. This theory cannot explain the phase shift which has been measured in the diurnal librations of Mimas. This speaks against a solid structure for Mimas, i.e. Mimas could have a global internal ocean.

Subject headings: Resonances, spin-orbit – Rotational dynamics – Satellites, shapes – Celestial mechanics – Saturn, satellites

1. Introduction

The Cassini space mission has given us invaluable data on the satellites of Saturn. In particular, we now dispose of measurements of their shapes as triaxial ellipsoids (Thomas 2010, e.g.), and the rotation of Janus, Epimetheus (Tiscareno et al. 2009), Mimas (Tajeddine et al. 2014), Enceladus (Thomas et al. 2016), and Titan (Stiles et al. 2008; Meriggiola et al. 2016) have been measured. An issue is to get clues on the interior from these informations.

Most of the natural satellites of the giant planets are expected to have reached a state of synchronous rotation, known as Cassini State. This is a dynamical equilibrium from which small departures are signatures of the internal structure. These small departures are longitudinal and latitudinal librations, the latter ones translating into an obliquity. The main part of the longitudinal librations is a periodic diurnal oscillation, named physical librations. For a rigid body, they read (Murray & Dermott 2000, Eq. 5.123, e.g.)

$$\gamma(t) = \frac{2e}{1-(n/\omega_0)^2}\sin(nt), \tag{1}$$

e being the orbital eccentricity of the satellite, n its orbital frequency, and ω_0 the frequency of the small proper oscillations around the equilibrium. We have:

$$\omega_0 = n\sqrt{3\frac{I_{22}-I_{11}}{I_{33}}G_{200}(e)}, \tag{2}$$

where the quantities I_{xx} are diagonal elements of the tensor of inertia of the satellite, and $G_{200}(e)$ is an eccentricity function made popular by Kaula (1966):

$$G_{200}(e) = 1 - \frac{5}{2}e^2 + \frac{13}{16}e^4 - \frac{35}{288}e^6 + \mathcal{O}(e^8). \tag{3}$$

This function is also known as the Hansen function $H(1,e)$, and is present in Cayley (1861).

The quantity $(I_{22}-I_{11})/I_{33}$, sometimes written as $(B-A)/C$, represents the equatorial ellipticity, or the triaxiality, of the distribution of mass inside the satellite. This formula assumes a rigid shape, i.e. the tensor of inertia is constant.

A seminal paper by Goldreich & Mitchell (2010) has shown that if the satellite is not strictly rigid, but viscoelastic, then a restoring torque tends to counterbalance the tidal torque of the parent planet, to lower the amplitude of the physical librations. This has motivated recent studies (Van Hoolst et al. 2013; Richard et al. 2014; Makarov et al. 2016), which revisit the theory of the librations in including a tidal parameter, k_2 or h_2, which characterizes the amplitude of variation of the gravity field, or of the surface, at the diurnal, or orbital, frequency n. In these studies, the body is assumed to be at the hydrostatic equilibrium.

The theory of the hydrostatic equilibrium tells us that the mass distribution in the body, i.e. its inertia, is shaped by its rotation and the tidal torque of its parent planet, while the inertia rules its rotation. However, in most of the studies, the inertia is mainly composed of a constant component which has no chance to be shaped by the rotation, while being assumed to correspond to the hydrostatic equilibrium.

In this paper I go further, in assuming that part of the mass distribution of these bodies is frozen, while part of it is still being shaped by the rotational and tidal deformation. For that, I first show from the measured radii that the departures from the hydrostatic equilibrium are ubiquitous in the system of Saturn (Sect. 2). Then I express the tensor of inertia of a satellite orbiting a giant planet, in considering a frozen triaxiality superimposed with elastic deformation (Sect 3). I then deduce the librational dynamics of the satellite (Sect. 4), which I apply to the specific cases of Epimetheus and Mimas, for which longitudinal librations have been measured, and which are assumed to have rigid structure. Finally, I introduce the dissipative part of the tides (Sect. 7), to investigate their influence

on the measurements. The reader can refer to Tab. 6 for the notations.

2. Departures from the hydrostatic equilibrium

Usually the shape of such a body is assumed to be the signature of an hydrostatic equilibrium. This means that the mass distribution is an equilibrium between the gravity of the body, and the rotational and tidal deformations it is subjected to. For a natural satellite orbiting a giant planet, it is assumed that the tidal deformation is only due to the planet, and that its spin rate is equal to its orbital rate, i.e. it rotates synchronously. This gives the following relations (Matsuyama & Nimmo 2009; Correia & Rodriguez 2013; Tricarico 2014):

$$\frac{\mathfrak{b}-\mathfrak{c}}{\mathfrak{a}-\mathfrak{c}} \approx \frac{1}{4} - \frac{495}{224}q + \frac{51}{32}e^2, \tag{4}$$

$$\frac{J_2}{C_{22}} \approx \frac{10}{3} - \frac{400}{21}q + \frac{34}{3}e^2, \tag{5}$$

$\mathfrak{a} > \mathfrak{b} > \mathfrak{c}$ being respectively the 3 planet-facing, orbit-facing, and polar radii, J_2 and C_{22} the classical Stokes coefficients, and $q = n^2R^3/(\mathcal{G}M)$. In this last formula, M is the mass of the satellite, and R its mean radius. The relation (4) holds for the shape, and (5) for the gravity field. The synchronous rotation results in a forcing of the triaxiality of the satellite, since it on average always presents the same face to its parent planet.

The Cassini mission has given us invaluable data on the shapes (Tab. 2) and gravity fields (Tab. 1) of some Saturnian satellites, and a comparison with the numbers predicted by the hydrostatic theory reveals some departure (Tab. 3), as for the Moon (Jeffreys 1937; Lambeck & Pullan 1980; Garrick-Bethell et al. 2014, e.g.) and Phobos (Le Maistre et al. 2013, e.g.).

EDITOR: PLACE TABLE 1 HERE.

EDITOR: PLACE TABLE 2 HERE.

EDITOR: PLACE TABLE 3 HERE.

These departures from the hydrostatic equilibrium may have different origins, such as a fossil shape, internal processes, or impacts... In the following, I consider them as frozen inertia.

3. The tensor of inertia

I consider a homogeneous, triaxial and synchronous satellite. Its orbital dynamics comes from the oblate two-body problem, i.e. the semimajor axis a and the eccentricity e are constant, and the mean longitude λ and longitude of the pericentre ϖ have a uniform precessional motion, the associated frequencies being n and $\dot{\varpi}$, respectively. Moreover, its orbit is assumed to lie in the equatorial plane of the planet, as a consequence the satellite has no obliquity. I also neglect the polar motion, the angular momentum of the satellite being collinear to its polar axis of inertia.

The tensor of inertia of the satellite $\mathcal{I}$ can be decomposed as:

$$\mathcal{I} = \mathcal{I}^{(f)} + \mathcal{I}^{(s)} + \mathcal{I}^{(t)} + \mathcal{I}^{(r)}, \tag{6}$$

where

- $\mathcal{I}^{(f)}$ is the frozen component. It is constant and its physical origin is here not addressed,

- $\mathcal{I}^{(s)}$ is the inertia of a spherical body. We have

$$I_{ij}^{(s)} = \iiint_{\text{body}} \rho(r) r^2 \, \mathrm{d}V \delta_{ij}, \tag{7}$$

  which gives, for our homogeneous body:

$$I_{ij}^{(s)} = \frac{2}{5} M R^2 \delta_{ij}, \tag{8}$$

  δ_{ij} being the classical Kronecker symbol, $\rho(r)$ the density at the distance r, and $\mathrm{d}V$ a volume element.

- $\mathcal{I}^{(t)}$ is the deformation of the inertia induced by the tides, and

- $\mathcal{I}^{(r)}$ is the rotational deformation.

In this section, I neglect the dissipative part of the deformation. As a consequence, the sum $\mathcal{I}^{(t)} + \mathcal{I}^{(r)}$ represents an elastic deformation, and will be denoted $\mathcal{I}^{(e)}$, e standing for *elastic*. The dissipation will be considered in the Sect. 7.

3.1. The frozen inertia

The frozen part of the tensor of inertia is constant. As a symmetric tensor, it can be written under a diagonal form in an appropriate reference frame $(\hat{f}_1, \hat{f}_2, \hat{f}_3)$, whose axes are the principal axes of inertia, i.e.:

$$\mathcal{I}^{(f)} = \begin{pmatrix} I_{11}^{(f)} & 0 & 0 \\ 0 & I_{22}^{(f)} & 0 \\ 0 & 0 & I_{33}^{(f)} \end{pmatrix}, \tag{9}$$

with $I_{11}^{(f)} \leq I_{22}^{(f)} \leq I_{33}^{(f)}$. In the literature dealing with rigid rotation, these 3 moments of inertia are often written A, B and C, respectively.

3.2. The elastic inertia

The elastic tensor $\mathcal{I}^{(e)}$ results from the combined action of the tidal torque of the parent planet and the rotation of the satellite. Following (Williams et al. 2001, e.g.), we have

$$I_{ij}^{(t)} = -k_2 \frac{M_{\wp} R^5}{r^3} \left(x_i x_j - \frac{\delta_{ij}}{3} \right), \tag{10}$$

and

$$I_{ij}^{(r)} = \frac{k_2 R^5}{3\mathcal{G}} \left(\omega_i \omega_j - \frac{n^2}{3} \delta_{ij} \right), \tag{11}$$

where $x_1 = x$, $x_2 = y$ and $x_3 = z$ are the coordinates of the unit vector pointing to the parent planet in the reference frame of the principal axes of inertia of the satellite. In this frame, $\vec{\omega} = \omega_1 \hat{f}_1 + \omega_2 \hat{f}_2 + \omega_3 \hat{f}_3$ is the rotation vector of the satellite. k_2 is the second order gravitational Love number, which characterizes the amplitude of deformation of the gravity field. $M_{\wp}$ is the mass of the parent planet, R is the mean radius of the satellite, and r is the distance between the barycentres of the planet and the satellite.

Our assumptions imply $x_3 = 0$, $\omega_1 = \omega_2 = 0$ and $\omega_3 = n$, this results in:

$$I_{11}^{(e)} = -k_2 \frac{M_{\wp} R^5}{3a^3} \left(1 + \left(\frac{a}{r} \right)^3 \left(2x^2 - y^2 \right) \right), \tag{12}$$

$$I_{12}^{(e)} = -k_2 \frac{M_{\wp} R^5}{r^3} xy, \tag{13}$$

$$I_{22}^{(e)} = -k_2 \frac{M_\saturn R^5}{3a^3} \left(1 + \left(\frac{a}{r}\right)^3 \left(2y^2 - x^2\right)\right), \tag{14}$$

$$I_{33}^{(e)} = k_2 \frac{M_\saturn R^5}{9a^3} \left(2 + 3\left(\frac{a}{r}\right)^3\right), \tag{15}$$

$$I_{13}^{(e)} = I_{23}^{(e)} = 0, \tag{16}$$

a being the semimajor axis of the satellite.

The coordinates of the parent planet x and y can now be expressed with respect to the orbital elements of the satellite and to its orientation. Since it is assumed to have only a longitudinal motion, its orientation is given by an instantaneous rotation angle p around $\hat{f}_3$ such that $\dot{p} = n$ and its origin $p = 0$ corresponds to a state in which the long axis of the satellite points to the barycenter of the parent planet.

In the reference frame $(\hat{f}_1, \hat{f}_2, \hat{f}_3)$, we have

$$\begin{pmatrix} x \\ y \\ z \end{pmatrix} = \begin{pmatrix} \cos p & \sin p & 0 \\ -\sin p & \cos p & 0 \\ 0 & 0 & 1 \end{pmatrix} \times \begin{pmatrix} \cos(f + \varpi) \\ \sin(f + \varpi) \\ 0 \end{pmatrix}, \tag{17}$$

where f stands for the true anomaly, and ϖ for the longitude of the pericenter. These quantities can be introduced in the formulae (12) to (15), before being expanded with respect to the eccentricity e using the classical formulae (Duriez 2002, Eq. 3.117), (Murray & Dermott 2000, Eq. 2.84 & 2.85):

$$\frac{a}{r} = 1 + 2\sum_{\nu=1}^{\infty} J_\nu(\nu e)\cos(\nu(\lambda - \varpi)), \tag{18}$$

$$\cos f = 2\frac{1-e^2}{e}\sum_{\nu=1}^{\infty} J_\nu(\nu e)\cos(\nu(\lambda - \varpi)) - e, \tag{19}$$

$$\sin f = 2\sqrt{1-e^2}\sum_{\nu=1}^{\infty} \frac{\mathrm{d}J_\nu(\nu e)}{\mathrm{d}e}\frac{\sin(\nu(\lambda - \varpi))}{\nu}, \tag{20}$$

where J_ν are the Bessel functions of the first kind. I now introduce the argument of the synchronous spin-orbit resonance $\sigma = p - \lambda + \pi$ (Henrard 2005, e.g.) and the mean anomaly $\mathcal{M} = \lambda - \varpi$ to get, up to the second order in the eccentricity:

$$\begin{aligned}
I_{11}^{(e)} &= k_2 \frac{M_\wp R^5}{a^3} \left(-\frac{5}{18} - \frac{e^2}{4} - \frac{1}{2}\left(1 - \frac{5}{2}e^2\right)\cos 2\sigma \right. \\
&\quad + \frac{e}{4}\left(\cos(\mathcal{M}+2\sigma) - 2\cos(\mathcal{M}) - 7\cos(\mathcal{M}-2\sigma)\right) \\
&\quad \left. - \frac{e^2}{4}\left(3\cos(2\mathcal{M}) + 17\cos(2\mathcal{M}-2\sigma)\right)\right), \qquad (21) \\
I_{12}^{(e)} &= \frac{k_2}{2}\frac{M_\wp R^5}{a^3} \left(\left(1 - \frac{5}{2}e^2\right)\sin 2\sigma - \frac{e}{2}\left(\sin(\mathcal{M}+2\sigma) + 7\sin(\mathcal{M}-2\sigma)\right) \right. \\
&\quad \left. - \frac{17}{2}e^2 \sin(2\mathcal{M}-2\sigma)\right), \qquad (22) \\
I_{22}^{(e)} &= k_2 \frac{M_\wp R^5}{a^3} \left(-\frac{5}{18} - \frac{e^2}{4} + \frac{1}{2}\left(1 - \frac{5}{2}e^2\right)\cos 2\sigma \right. \\
&\quad + \frac{e}{4}\left(7\cos(\mathcal{M}-2\sigma) - \cos(\mathcal{M}+2\sigma) - 2\cos(\mathcal{M})\right) \\
&\quad \left. + \frac{e^2}{4}\left(17\cos(2\mathcal{M}-2\sigma) - 3\cos(2\mathcal{M})\right)\right), \qquad (23) \\
I_{33}^{(e)} &= k_2 \frac{M_\wp R^5}{a^3} \left(\frac{5}{9} + \frac{1}{2}e^2 + e\cos(\mathcal{M}) + \frac{3}{2}e^2\cos(2\mathcal{M})\right). \qquad (24)
\end{aligned}$$

The argument of the spin-orbit resonance σ is usually set to 0, except in (Correia & Rodriguez 2013, Eq. 37-38). Here, I keep σ as a variable, since it will be involved in the equation of the librations. Since the rotation is assumed to shape the inertia, and the inertia rules the rotation, then σ should be let free to vary. I will anyway assume that the frequency associated with σ is null, i.e. I assume σ to be constant on average, which is consistent with the resonant locking. The formulae (21) to (24) imply that the tidal response of the satellite does not depend on the frequency of the excitation. Actually the tidal parameter is frequency-dependent. To model this dependency I define the following frequencies:

$$\nu_0 = 0, \tag{25}$$

$$\nu_1 = |n - \dot{\varpi}|, \tag{26}$$

$$\nu_2 = |2n - 2\dot{\varpi}|, \tag{27}$$

and the elastic tensor of inertia becomes:

$$\begin{aligned} I_{11}^{(e)} &= \frac{M_\hbar R^5}{a^3}\left(k_2(\nu_0)\left(-\frac{5}{18}-\frac{e^2}{4}-\frac{1}{2}\left(1-\frac{5}{2}e^2\right)\cos 2\sigma\right)\right. \\ &\quad +k_2(\nu_1)\frac{e}{4}\left(\cos(\mathcal{M}+2\sigma)-2\cos(\mathcal{M})-7\cos(\mathcal{M}-2\sigma)\right) \\ &\quad \left.-k_2(\nu_2)\frac{e^2}{4}\left(3\cos(2\mathcal{M})+17\cos(2\mathcal{M}-2\sigma)\right)\right), \end{aligned} \tag{28}$$

$$\begin{aligned} I_{12}^{(e)} &= \frac{M_\hbar R^5}{2a^3}\left(k_2(\nu_0)\left(1-\frac{5}{2}e^2\right)\sin 2\sigma - k_2(\nu_1)\frac{e}{2}\left(\sin(\mathcal{M}+2\sigma)+7\sin(\mathcal{M}-2\sigma)\right)\right. \\ &\quad \left.-\frac{17}{2}e^2 k_2(\nu_2)\sin(2\mathcal{M}-2\sigma)\right), \end{aligned} \tag{29}$$

$$\begin{aligned} I_{22}^{(e)} &= \frac{M_\hbar R^5}{a^3}\left(k_2(\nu_0)\left(-\frac{5}{18}-\frac{e^2}{4}+\frac{1}{2}\left(1-\frac{5}{2}e^2\right)\cos 2\sigma\right)\right. \\ &\quad +\frac{e}{4}k_2(\nu_1)\left(7\cos(\mathcal{M}-2\sigma)-\cos(\mathcal{M}+2\sigma)-2\cos(\mathcal{M})\right) \\ &\quad \left.+\frac{e^2}{4}k_2(\nu_2)\left(17\cos(2\mathcal{M}-2\sigma)-3\cos(2\mathcal{M})\right)\right), \end{aligned} \tag{30}$$

$$I_{33}^{(e)} = \frac{M_\hbar R^5}{a^3}\left(k_2(\nu_0)\left(\frac{5}{9}+\frac{1}{2}e^2\right)+ek_2(\nu_1)\cos(\mathcal{M})+\frac{3}{2}e^2k_2(\nu_2)\cos(2\mathcal{M})\right). \tag{31}$$

In the literature, $k_2(\nu_0)$ is sometimes denoted as the fluid, or secular, Love number k_f. It represents an indefinitely slow deformation. However, $k_2(\nu_1)$ and $k_2(\nu_2)$ are often assumed to be equal and denoted as k_2. The periods of the deformations associated are respectively the orbital and half the orbital ones, which are also the diurnal and semi-diurnal periods of the satellite.

4. The librational dynamics

4.1. The librational equations

The gravitational torque of the parent planet, which acts on the satellite, is collinear to the polar axis, since we consider a planar orbit. Its non-null component Γ reads (Williams et al. 2001, e.g.):

$$\Gamma = 3\frac{\mathcal{G}M_{\hbar}}{r^3}\left((I_{22}-I_{11})xy + I_{12}(x^2-y^2)\right). \tag{32}$$

After expansion with respect to the orbital elements, I get, up to the second order in the eccentricity:

$$\begin{aligned}\Gamma &= \left(-\frac{3}{2}+\frac{15}{4}e^2\right)\left(I_{22}-I_{11}\right)^{(f)} n^2 \sin 2\sigma + \frac{3}{4}\left(I_{22}-I_{11}\right)^{(f)} en^2\left(\sin(\mathcal{M}+2\sigma)+7\sin(\mathcal{M}-2\sigma)\right)\\ &+\frac{51}{4}\left(I_{22}-I_{11}\right)^{(f)} e^2n^2\sin(2\mathcal{M}-2\sigma) + 6en^2\frac{M_{\hbar}R^5}{a^3}\left(k_f-k_2(\nu_1)\right)\sin\mathcal{M}\\ &+\frac{51}{4}n^2e^2\frac{M_{\hbar}R^5}{a^3}\left(k_f-k_2(\nu_2)\right)\sin 2\mathcal{M},\end{aligned} \tag{33}$$

while Γ is also the time-derivative of the norm of the angular momentum. This yields

$$\Gamma = \frac{d(I_{33}\dot{p})}{dt}, \tag{34}$$

i.e.

$$\begin{aligned}\Gamma &= \left(\frac{2}{5}MR^2 + \frac{M_{\hbar}R^5}{a^3}\left(k_f\left(\frac{5}{9}+\frac{1}{2}e^2\right)+ek_2(\nu_1)\cos\mathcal{M}+\frac{3}{2}e^2k_2(\nu_2)\cos 2\mathcal{M}\right)\right)\ddot{\sigma}\\ &-\frac{M_{\hbar}R^5}{a^3}(n-\dot{\varpi})\left(k_2(\nu_1)e\sin\mathcal{M}+3k_2(\nu_2)e^2\sin 2\mathcal{M}\right)\dot{\sigma}.\end{aligned} \tag{35}$$

The frozen component of I_{33}, i.e. $I_{33}^{(f)}$, should appear in this equation, but since I_{33} is not affected by σ, then its secular part has the same behavior than its frozen part, distinguishing it is in that specific case useless. So, it is kind of absorbed in $\frac{2}{5}MR^2 + \frac{M_\hbar R^5}{a^3}k_f\left(\frac{5}{9}+\frac{1}{2}e^2\right)$.

In equating the formula (33) with the (35), I get the differential equation ruling the longitudinal libration of the satellite, i.e.

$$\begin{aligned} & K_1\sin 2\sigma + K_2\sin(\mathcal{M}+2\sigma) + K_3\sin(\mathcal{M}-2\sigma) + K_4\sin(2\mathcal{M}-2\sigma) + K_5\sin\mathcal{M} + K_6\sin 2\mathcal{M} \\ = \;& K_7\ddot{\sigma} + K_8\ddot{\sigma}\cos\mathcal{M} + K_9\ddot{\sigma}\cos 2\mathcal{M} + K_{10}\dot{\sigma}\sin\mathcal{M} + K_{11}\dot{\sigma}\sin 2\mathcal{M} \end{aligned} \tag{36}$$

with

$$K_1 = \left(-\frac{3}{2}+\frac{15}{4}e^2\right)(I_{22}-I_{11})^{(f)}n^2, \tag{37}$$

$$K_2 = \frac{3}{4}(I_{22}-I_{11})^{(f)}en^2, \tag{38}$$

$$K_3 = \frac{21}{4}(I_{22}-I_{11})^{(f)}en^2 = 7K_2, \tag{39}$$

$$K_4 = \frac{51}{4}(I_{22}-I_{11})^{(f)}e^2n^2, \tag{40}$$

$$K_5 = 6en^2\frac{M_\hbar R^5}{a^3}\left(k_f - k_2(\nu_1)\right), \tag{41}$$

$$K_6 = \frac{51}{4}e^2n^2\frac{M_\hbar R^5}{a^3}\left(k_f - k_2(\nu_2)\right), \tag{42}$$

$$K_7 = \frac{2}{5}MR^2 + \frac{M_\hbar R^5}{a^3}k_f\left(\frac{5}{9}+\frac{e^2}{2}\right), \tag{43}$$

$$K_8 = \frac{M_\hbar R^5}{a^3}ek_2(\nu_1), \tag{44}$$

$$K_9 = \frac{3}{2}\frac{M_\hbar R^5}{a^3}e^2k_2(\nu_2), \tag{45}$$

$$K_{10} = -\frac{M_\hbar R^5}{a^3}(n-\dot{\varpi})ek_2(\nu_1), \tag{46}$$

$$K_{11} = -3\frac{M_{\hbar} R^5}{a^3}(n - \dot{\varpi})e^2 k_2(\nu_2). \quad (47)$$

4.2. The librational solution

The equation (36) can be simplified for an analytical resolution in neglecting the variations of σ with respect to the ones of $\mathcal{M}$, and $\dot{\sigma}$. It becomes:

$$\ddot{\sigma} + \omega_0^2 \sigma = \kappa_1 \sin \mathcal{M}, \quad (48)$$

with

$$\omega_0^2 = \left(3 - \frac{15}{2}e^2\right) n^2 \frac{(I_{22} - I_{11})^{(f)}}{\frac{2}{5}MR^2 + k_f \left(\frac{5}{9} + \frac{e^2}{2}\right) M_{\hbar} \frac{R^5}{a^3}}, \quad (49)$$

$$\kappa_1 = 6en^2 \frac{(I_{22} - I_{11})^{(f)} + M_{\hbar} \frac{R^5}{a^3} (k_f - k_2(\nu_1))}{\frac{2}{5}MR^2 + k_f \left(\frac{5}{9} + \frac{e^2}{2}\right) M_{\hbar} \frac{R^5}{a^3}}, \quad (50)$$

and this results in

$$\sigma(t) = \frac{\kappa_1}{\omega_0^2 - (n - \dot{\varpi})^2} \sin \mathcal{M}, \quad (51)$$

after damping of the proper oscillations, their frequency being ω_0. Here the semi-diurnal oscillations have been dropped. The numerical application shows that their amplitude is negligible.

The Tab. 4 proposes a comparison between this study and two previous ones, by Van Hoolst et al. (2013) and Richard et al. (2014). These two studies aimed at modeling the librations of a satellite composed of a viscoelastic crust coating a global ocean, itself enshrouding a rigid core. Hence, they consider pressure and gravitational couplings between

the different layers, that I do not have here. In considering only the outer shell in their studies, I managed to get equations like my Eq. (48), from (Van Hoolst et al. 2013, Eq. 45) and (Richard et al. 2014, App. A), with the help of (Richard 2014).

EDITOR: PLACE TABLE 4 HERE.

In those two studies, A, B and C stand for the mean values of the diagonal elements of the tensor of inertia $\mathcal{I}$, i.e. I_{11}, I_{22} and I_{33}. Moreover, the triaxiality is supposed to be entirely due to the rotational and tidal deformations, i.e. there is no frozen component in $(I_{22}-I_{11})$, and the second degree in the eccentricity has been neglected. In (Van Hoolst et al. 2013), k_2 stands for $k_2(\nu_1)$, while in (Richard et al. 2014), the topographical Love number h_2 has been used.

My formula for ω_0 is consistent with the one of Richard et al. (2014), while Van Hoolst et al. (2013) have a signature of the tidal deformation at the diurnal frequency. However, these two previous studies are consistent with each other for the coefficient κ_1 for $h_2 = 5k_2/3$.

A difference between these studies and mine is that they assume the resonant argument σ to be fixed to 0 in the expression of the tensor of inertia (Eq. 28 to 30), while it is a variable of the problem. If we set $\sigma = 0$ in the tensor of inertia, then the gravitational torque Γ defined by the Eq. 32 becomes, after averaging over the mean anomaly $\mathcal{M}$:

$$\Gamma = 3\frac{\mathcal{G}M_{\text{ħ}}}{r^3}\left(I_{22}^{(f)} - I_{11}^{(f)}\right)\sin 2\sigma \tag{52}$$

i.e. only the frozen component remains on average. If we had only an elastic inertia, then the average torque would be

$$\Gamma = 3\frac{\mathcal{G}M_{\hbar}}{r^3}\left(k_f M_{\hbar}\frac{R^5}{a^3}\cos 2\sigma \sin 2\sigma - k_f M_{\hbar}\frac{R^5}{a^3}\cos 2\sigma \sin 2\sigma\right) = 0, \tag{53}$$

that comes from

$$\begin{aligned} xy &= \frac{\sin 2\sigma}{2} + \mathcal{O}(e), & (54)\\ (I_{22} - I_{11})^{(e)} &= k_f M_{\hbar}\frac{R^5}{a^3}\cos 2\sigma + \mathcal{O}(e), & (55)\\ x^2 - y^2 &= \cos 2\sigma + \mathcal{O}(e), & (56)\\ I_{12}^{(e)} &= -\frac{k_f}{2}M_{\hbar}\frac{R^5}{a^3}\sin 2\sigma + \mathcal{O}(e). & (57) \end{aligned}$$

So, a frozen component in $(I_{22} - I_{11})$ is needed to get a non-null mean gravitational torque.

5. Modeling the tides

5.1. The Maxwell model

The classical Maxwell model (Karato 2008, e.g.) gives a pretty good estimation of the frequency-dependency of k_2. It depends on one parameter, the Maxwell time $\tau_M = \eta/\mu$, η being the viscosity and μ the rigidity. The complex Love number k_2^* reads

$$k_2^* = k_f \frac{J^*(\nu)}{J^*(\nu) + A_2/\mu} \tag{58}$$

with

$$A_2 = \frac{19}{2}\frac{\mu}{\rho g R}, \tag{59}$$

and J^* is the complex compliance defined as:

$$J^* = \frac{\nu\tau_M - \imath}{\mu\nu\tau_M}, \tag{60}$$

ν being the tidal frequency, and g the surface gravity of the body. k_2 is the real part of k_2^*, i.e.

$$\Re(k_2^*) = k_f \frac{1 + (1 + A_2)\nu^2\tau_M^2}{1 + (1 + A_2)^2\nu^2\tau_M^2}. \tag{61}$$

5.2. An improvement at high frequencies

At high frequencies, the Maxwell model lacks accuracy because it does not render the fact that anelasticity dominates viscoelasticity, i.e. the response of the material is not instantaneous anymore. The Andrade model is therefore more appropriate. This is the reason why Efroimsky (2012a) proposed the so-called Andrade-Maxwell model, that corresponds to the Andrade model at high frequencies and to the Maxwell model at lower frequencies. Its complex compliance reads:

$$\bar{J}(\nu) = \left(1 + (\imath\nu\tau_A)^{-N}\,\Gamma(1+N) - \imath\,(\nu\tau_M)^{-1}\right)/\mu, \tag{62}$$

Γ being the classical Γ function defined as

$$\Gamma(1+N) = \int_0^{+\infty} z^N e^{-z}\,\mathrm{d}z. \tag{63}$$

We can see that this model depends on 3 tidal parameters, which are the Maxwell time τ_M, an Andrade time τ_A that has been introduced by Efroimsky (2012a, Eq. 78), and an Andrade parameter N. The Andrade time should be equal to the Maxwell time to have a continuous transition between viscoelasticy and anelasticity, i.e. $\tau_A = \tau_M$. N is usually

assumed to lie between 0.1 and 0.5, I will take the classical value $N = 0.3$. The resulting expression for the Andrade-Maxwell model is

$$\Re(k_2^*) = k_f \frac{\mathcal{A}^2 + \mathcal{A}A_2 + \mathcal{B}^2}{\mathcal{A}^2 + 2\mathcal{A}A_2 + A_2^2 + \mathcal{B}^2} \tag{64}$$

with

$$\mathcal{A} = 1 + (\nu\tau_A)^{-N} \cos\left(\frac{N\pi}{2}\right) \Gamma(1+N), \tag{65}$$

$$\mathcal{B} = (\nu\tau_M)^{-1} + (\nu\tau_A)^{-N} \sin\left(\frac{N\pi}{2}\right) \Gamma(1+N). \tag{66}$$

The Andrade parameter τ_A is an order of magnitude of the period above which the excitation will generate the Andrade creep, responsible for anelasticity. Setting τ_A to the infinity renders the Maxwell rheology.

The Fig. 1 illustrates the elastic tides given by these two models, for Mimas and Epimetheus, in using the physical parameters given in Tab. 5.

EDITOR: PLACE FIGURE 1 HERE.

6. Application to Epimetheus and Mimas

Diurnal librations have been measured for Epimetheus and Mimas, thanks to Cassini data (Tiscareno et al. 2009; Tajeddine et al. 2014). These two bodies are a priori assumed to be solid bodies, which legitimates the use of this model to explain their librations.

6.1. Methodology

A numerical integration of the Eq.(36) is performed, with the 10th order Adams-Bashforth-Moulton predictor-corrector scheme. A frequency analysis is then made to decompose the variable $\sigma(t)$ under a quasi-periodic formulation. This way, the proper oscillations and the forced ones are clearly identified. The frequency analysis algorithm is based on Laskar's original idea (Laskar 1999, 2005), has been adapted for the rotational dynamics by Noyelles et al. (2008), and used many times since. The initial conditions of the numerical integration are given by the analytical solution at $t = 0$, i.e. the Eq.(51) and its time-derivative, while the parameters are gathered in Tab. 5.

For each of these satellites, several simulations are run, which differ by the fraction of non-hydrostaticity. This starts from the formula giving the mean value of $I_{22} - I_{11}$:

$$< I_{22} - I_{11} > \approx (I_{22} - I_{11})^{(f)} + k_f \frac{M_\wp R^5}{a^3} \cos 2 < \sigma >, \tag{67}$$

and then, two approaches are considered:

1. either the secular Love number k_f is set to be constant. I first set it to 1.5 before discussing the implications of a smaller k_f, which could be more physically relevant. I define the parameter α such that

$$(I_{22} - I_{11})^{(f)} = \alpha k_f \frac{M_\wp R^5}{a^3}. \tag{68}$$

   This approach suggests that the body is composed of the superimposition of 2 mass distributions, an elastic and a frozen ones. The elastic contribution is fully consistent with the hydrostatic theory, and the frozen contribution supplements the elastic one, as an excess of triaxiality. This excess represents a fraction α of the elastic contribution,

2. or the mean value of $(I_{22} - I_{11})$ is considered to be constant and determined from the shape of the satellite in assuming a constant density, i.e.

$$< I_{22} - I_{11} >= \frac{M}{5} \left(\mathfrak{a}^2 - \mathfrak{b}^2 \right), \tag{69}$$

which implies

$$< C_{22} >= \frac{\mathfrak{a}^2 - \mathfrak{b}^2}{20R^2}. \tag{70}$$

I define the parameter β such that

$$(I_{22} - I_{11})^{(f)} = \beta \frac{M}{5} \left(\mathfrak{a}^2 - \mathfrak{b}^2 \right), \tag{71}$$

and k_f is obtained from the formula (67). This would mean that the mean inertia of the body is consistent with the hydrostatic theory, but part of this inertia is frozen, the remaining part being still elastic.

EDITOR: PLACE TABLE 5 HERE.

6.2. Epimetheus

For Epimetheus, a physical libration of $5.9 \pm 1.2°$ has been measured by Tiscareno et al. (2009). Such a large number is due to the triaxiality of the satellite, which makes the frequency of the proper oscillations ω_0 close to the orbital one, resulting in a large amplitude of response (Noyelles 2010, Fig. 6).

EDITOR: PLACE FIGURE 2 HERE.

The simulations with an excess of triaxiality result in a larger C_{22} (Fig. 2) than anticipated by the measured shape, but permit to reach the measured amplitude for $\alpha = 1.21^{+0.06}_{-0.09}$.

EDITOR: PLACE FIGURE 3 HERE.

$k_f = 1.5$ for the elastic part should be seen as an incomplete model, in the sense that no rigidity is considered. The Fig. 3 displays α for smaller values of k_f. In particular, we have $\alpha = 1.82^{+0.08}_{-0.11}$ for $k_f = 1$.

These numbers should be balanced by the uncertainties of a few kilometers on the radii $\mathfrak{a}$ and $\mathfrak{b}$, and some departures from an actual triaxial shape. We can also see that the analytical formulae for ω_0 (Eq. 49) and the amplitude 1 (Eq. 51) are validated by the numerical simulations.

EDITOR: PLACE FIGURE 4 HERE.

The simulations assuming a constant triaxiality for Epimetheus (Fig. 4) still validate the analytical formulae for ω_0 and the diurnal amplitude. Moreover, they do not result in a large enough amplitude to match the observed libration.

This study assumes that Epimetheus is triaxial. Actually the visual aspect of Epimetheus suggests significant departure from the ellipsoid. To the best of my knowledge, no higher order shape model has been published, this is why I assume the triaxial ellipsoid as a good enough model. Of course, the departures to the triaxiality should contribute to the librations.

6.3. Mimas

Tajeddine et al. (2014) have measured from Cassini data a surprisingly high diurnal amplitude for Mimas of 50.3 ± 1.0 arcmin, while a theoretical study by Noyelles et al. (2011) predicted half this number. That study assumed Mimas to be a rigid body made of a mixture of ice and silicates, with a radial gradient of porosity. It was modeled as two homogeneous layers, the inner one being denser than the outer one. Tajeddine et al. (2014) tested 5 plausible interiors to explain their measurements, and kept only two: Mimas had either a global ocean beneath an icy crust, or a highly elongated core of pretty heavy elements. This last explanation would be consistent with a model of formation of the Saturnian satellites proposed by Charnoz et al. (2011). In that scenario, the satellites would have been formed as droplets from the rings before migrating outward to their present location. The highly triaxial shape of the core would be the signature of a former more rapid rotation, itself meaning that the shape froze when Mimas was closer to Saturn than it is now. It translates into an excess of triaxiality.

EDITOR: PLACE FIGURE 5 HERE.

EDITOR: PLACE FIGURE 6 HERE.

The two figures 5 and 7 still validate the analytical formulae for ω_0 and the diurnal amplitude. Moreover, they permit the measured amplitude for $\alpha = 0.6225 \pm 0.0235$ and $k_f = 1.5$, while a constant C_{22} prohibits it. $k_f = 1$ would imply $\alpha = 1.2954 \pm 0.0332$ (Fig. 6).

EDITOR: PLACE FIGURE 7 HERE.

7. Influence of the creep

I now introduce the imaginary part of the Love number, that is often denoted as $\Im(k_2^*) = -k_2/Q$, where Q is a dissipation function. This imaginary part introduces a dissipation as a lag between the gravitational excitation of the parent planet and the response of the satellite. This lag depends on the tidal frequency, this is why this effect will appear as $\left(\frac{k_2}{Q}\right)(\nu)$.

7.1. Equations of the problem

As shown for instance in (Williams & Boggs 2015), the dissipative tide can be introduced in replacing in the formulae (28) to (31) $k_2\cos$ by $k_2\cos + k_2/Q\sin$ and $k_2\sin$ by $k_2\sin - k_2/Q\cos$. This geometrically means that the parent planet raises two bulges at the surface of the satellite, i.e. a bulge which is aligned with the direction of the planet, and which is responsible for the elastic tide, and a bulge in quadrature, which is responsible for the dissipative tide (Zahn 1966; Efroimsky 2012b, e.g.). The elastic inertia $\mathfrak{I}^{(e)}$ is replaced by a viscoelastic one $\mathfrak{I}^{(v)}$. This yields:

$$\begin{aligned}
I_{11}^{(v)} &= \frac{M_\eth R^5}{a^3}\left(k_2(\nu_0)\left(-\frac{5}{18}-\frac{e^2}{4}-\frac{1}{2}\left(1-\frac{5}{2}e^2\right)\cos 2\sigma\right)\right.\\
&\quad +k_2(\nu_1)\frac{e}{4}\left(\cos(\mathcal{M}+2\sigma)-2\cos(\mathcal{M})-7\cos(\mathcal{M}-2\sigma)\right)\\
&\quad +\left(\frac{k_2}{Q}\right)(\nu_1)\frac{e}{4}\left(\sin(\mathcal{M}+2\sigma)-2\sin(\mathcal{M})-7\sin(\mathcal{M}-2\sigma)\right)\\
&\quad -k_2(\nu_2)\frac{e^2}{4}\left(3\cos(2\mathcal{M})+17\cos(2\mathcal{M}-2\sigma)\right)\\
&\quad \left.-\left(\frac{k_2}{Q}\right)(\nu_2)\frac{e^2}{4}\left(3\sin(2\mathcal{M})+17\sin(2\mathcal{M}-2\sigma)\right)\right), \qquad (72)\\
I_{12}^{(v)} &= \frac{M_\eth R^5}{2a^3}\left(k_2(\nu_0)\left(1-\frac{5}{2}e^2\right)\sin 2\sigma - k_2(\nu_1)\frac{e}{2}\left(\sin(\mathcal{M}+2\sigma)+7\sin(\mathcal{M}-2\sigma)\right)\right.
\end{aligned}$$

$$
\begin{aligned}
&+\left(\frac{k_2}{Q}\right)(\nu_1)\frac{e}{2}\left(\cos(\mathcal{M}+2\sigma)+7\cos(\mathcal{M}-2\sigma)\right)\\
&-\frac{17}{2}e^2\left(k_2(\nu_2)\sin(2\mathcal{M}-2\sigma)-\left(\frac{k_2}{Q}\right)(\nu_2)\cos(2\mathcal{M}-2\sigma)\right)\Bigg), \qquad (73)\\
I_{22}^{(v)} &= \frac{M_\eth R^5}{a^3}\left(k_2(\nu_0)\left(-\frac{5}{18}-\frac{e^2}{4}+\frac{1}{2}\left(1-\frac{5}{2}e^2\right)\cos 2\sigma\right)\right.\\
&+\frac{e}{4}k_2(\nu_1)\left(7\cos(\mathcal{M}-2\sigma)-\cos(\mathcal{M}+2\sigma)-2\cos(\mathcal{M})\right)\\
&+\frac{e}{4}\left(\frac{k_2}{Q}\right)(\nu_1)\left(7\sin(\mathcal{M}-2\sigma)-\sin(\mathcal{M}+2\sigma)-2\sin(\mathcal{M})\right)\\
&+\frac{e^2}{4}k_2(\nu_2)\left(17\cos(2\mathcal{M}-2\sigma)-3\cos(2\mathcal{M})\right) \qquad (74)\\
&\left.+\frac{e^2}{4}\left(\frac{k_2}{Q}\right)(\nu_2)\left(17\sin(2\mathcal{M}-2\sigma)-3\sin(2\mathcal{M})\right)\right), \qquad (75)\\
I_{33}^{(v)} &= \frac{M_\eth R^5}{a^3}\left(k_2(\nu_0)\left(\frac{5}{9}+\frac{1}{2}e^2\right)+e\left(k_2(\nu_1)\cos(\mathcal{M})+\left(\frac{k_2}{Q}\right)(\nu_1)\sin(\mathcal{M})\right)\right.\\
&\left.+\frac{3}{2}e^2\left(k_2(\nu_2)\cos(2\mathcal{M})+\left(\frac{k_2}{Q}\right)(\nu_2)\sin(2\mathcal{M})\right)\right). \qquad (76)
\end{aligned}
$$

If we consider the Maxwell rheology, then the quantity $k_2/Q = -\Im(k_2^*)$ is obtained from the formula (58), i.e.

$$\left(\frac{k_2}{Q}\right)(\nu) = k_f\frac{A_2\nu\tau_M}{1+(1+A_2)^2\nu^2\tau_M^2}. \qquad (77)$$

It is in particular expected from any rheology that k_2/Q is null at the zero frequency, i.e. no dissipation occurs for a constant excitation.

The gravitational torque Γ (Eq. 33) then becomes

$$
\begin{aligned}
\Gamma &= 18n^2e^2\frac{M_\eth R^5}{a^3}\left(\frac{k_2}{Q}\right)(\nu_1)+\left(-\frac{3}{2}+\frac{15}{4}e^2\right)(I_{22}-I_{11})^{(f)}\,n^2\sin 2\sigma\\
&+\frac{3}{4}(I_{22}-I_{11})^{(f)}\,en^2\left(\sin(\mathcal{M}+2\sigma)+7\sin(\mathcal{M}-2\sigma)\right)\\
&+\frac{51}{4}(I_{22}-I_{11})^{(f)}\,e^2n^2\sin(2\mathcal{M}-2\sigma)+6en^2\frac{M_\eth R^5}{a^3}\left(k_f-k_2(\nu_1)\right)\sin\mathcal{M}
\end{aligned}
$$

$$+6en^2\frac{M_\hbar R^5}{a^3}\left(\frac{k_2}{Q}\right)(\nu_1)\cos\mathcal{M}$$
$$+\frac{51}{4}n^2e^2\frac{M_\hbar R^5}{a^3}\left(k_f-k_2(\nu_2)\right)\sin 2\mathcal{M}+\frac{51}{4}n^2e^2\frac{M_\hbar R^5}{a^3}\left(\frac{k_2}{Q}\right)(\nu_2)\cos 2\mathcal{M}, \quad (78)$$

that should be equated with:

$$\begin{aligned}\Gamma &= \left(\frac{2}{5}MR^2+\frac{M_\hbar R^5}{a^3}\left(k_f\left(\frac{5}{9}+\frac{1}{2}e^2\right)+ek_2(\nu_1)\cos\mathcal{M}+\frac{3}{2}e^2k_2(\nu_2)\cos 2\mathcal{M}\right)\right.\\
&\left.+e\left(\frac{k_2}{Q}\right)(\nu_1)\sin\mathcal{M}+\frac{3}{2}e^2\left(\frac{k_2}{Q}\right)(\nu_2)\sin 2\mathcal{M}\right)\ddot{\sigma}\\
&-\frac{M_\hbar R^5}{a^3}(n-\dot{\varpi})\left(k_2(\nu_1)e\sin\mathcal{M}+3k_2(\nu_2)e^2\sin 2\mathcal{M}\right.\\
&\left.-\left(\frac{k_2}{Q}\right)(\nu_1)e\cos\mathcal{M}-3\left(\frac{k_2}{Q}\right)(\nu_2)e^2\cos 2\mathcal{M}\right)\dot{\sigma}, \quad (79)\end{aligned}$$

to give the following equation, ruling the libration of the satellite:

$$\begin{aligned}&K_0+K_1\sin 2\sigma+K_2\sin(\mathcal{M}+2\sigma)+K_3\sin(\mathcal{M}-2\sigma)+K_4\sin(2\mathcal{M}-2\sigma)\\
&+K_5\sin\mathcal{M}+K_6\sin 2\mathcal{M}+K_{12}\cos\mathcal{M}+K_{13}\cos 2\mathcal{M}\\
=\;&K_7\ddot{\sigma}+K_8\ddot{\sigma}\cos\mathcal{M}+K_9\ddot{\sigma}\cos 2\mathcal{M}+K_{10}\dot{\sigma}\sin\mathcal{M}+K_{11}\dot{\sigma}\sin 2\mathcal{M}\\
&+K_{14}\ddot{\sigma}\sin\mathcal{M}+K_{15}\ddot{\sigma}\sin 2\mathcal{M}+K_{16}\dot{\sigma}\cos\mathcal{M}+K_{17}\dot{\sigma}\cos 2\mathcal{M}, \quad (80)\end{aligned}$$

with

$$K_0 = 18n^2e^2\frac{M_\hbar R^5}{a^3}\left(\frac{k_2}{Q}\right)(\nu_1), \quad (81)$$
$$K_{12} = 6en^2\frac{M_\hbar R^5}{a^3}\left(\frac{k_2}{Q}\right)(\nu_1), \quad (82)$$
$$K_{13} = \frac{51}{4}e^2n^2\frac{M_\hbar R^5}{a^3}\left(\frac{k_2}{Q}\right)(\nu_2), \quad (83)$$

$$K_{14} = \frac{M_\hbar R^5}{a^3} e \left(\frac{k_2}{Q}\right)(\nu_1), \tag{84}$$

$$K_{15} = \frac{3}{2}\frac{M_\hbar R^5}{a^3} e^2 \left(\frac{k_2}{Q}\right)(\nu_2), \tag{85}$$

$$K_{16} = \frac{M_\hbar R^5}{a^3}(n-\dot{\varpi}) e \left(\frac{k_2}{Q}\right)(\nu_1), \tag{86}$$

$$K_{17} = 3\frac{M_\hbar R^5}{a^3}(n-\dot{\varpi}) e^2 \left(\frac{k_2}{Q}\right)(\nu_2), \tag{87}$$

the other K_i being the same as in the conservative case (Eq. 37 to 47).

7.2. Librational solution

As before, the Eq.(80) can be simplified into

$$\ddot{\sigma} + \omega_0^2 \sigma = \kappa_0 + \kappa_1 \sin\mathcal{M} + \kappa_2 \cos\mathcal{M}, \tag{88}$$

with

$$\kappa_0 = \frac{18 e^2 M_\hbar \frac{R^5}{a^3}\left(\frac{k_2}{Q}\right)(\nu_1)}{\frac{2}{5}MR^2 + \frac{M_\hbar R^5}{a^3} k_f \left(\frac{5}{9} + \frac{e^2}{2}\right)}, \tag{89}$$

$$\kappa_2 = \frac{6 e M_\hbar \frac{R^5}{a^3}\left(\frac{k_2}{Q}\right)(\nu_1)}{\frac{2}{5}MR^2 + \frac{M_\hbar R^5}{a^3} k_f \left(\frac{5}{9} + \frac{e^2}{2}\right)}, \tag{90}$$

$$\tag{91}$$

ω_0 and κ_1 being defined as before (Eq.49 & 50). This results in:

$$\sigma(t) = \frac{\kappa_0}{\omega_0^2} + \frac{\kappa_1}{\omega_0^2 - (n-\dot{\varpi})^2}\sin\mathcal{M} + \frac{\kappa_2}{\omega_0^2 - (n-\dot{\varpi})^2}\cos\mathcal{M}. \tag{92}$$

This formula can be also written as

$$\sigma(t) = \sigma_0 + \sigma_1 \sin(\mathcal{M} + \phi_1), \tag{93}$$

with

$$\sigma_0 = \frac{6e^2 M_\hbar \frac{R^5}{a^3} \left(\frac{k_2}{Q}\right)(\nu_1)}{\left(1 - \frac{5}{2}e^2\right)(I_{22} - I_{11})^{(f)}}, \tag{94}$$

$$\sigma_1 = \frac{\sqrt{\kappa_1^2 + \kappa_3^2}}{\omega_0^2 - (n - \dot{\varpi})^2}, \tag{95}$$

$$\tan\phi_1 = \frac{M_\hbar \frac{R^5}{a^3} \left(\frac{k_2}{Q}\right)(\nu_1)}{(I_{22} - I_{11})^{(f)} + M_\hbar \frac{R^5}{a^3}(k_f - k_2(\nu_1))}. \tag{96}$$

We can see that the dissipative tide shifts the phase of the libration, not only in the periodic term, but also in adding a constant term that corresponds to the expected lag.

Until recently, this dissipation was considered only for the Moon. Williams et al. (2001) denoted the libration as τ and the constant lag σ_0 as $\Delta\tau$, its formulation being given by the Eq. (34a) in *Ibid.*. Their formulation is equivalent to mine provided that

1. the expansion is limited to the order 2 in the eccentricity,
2. their k_2/Q is my $(k_2/Q)(\nu_1)$,
3. their mean triaxiality is only due a frozen component, i.e. their $(B - A)$ is my $(I_{22} - I_{11})^{(f)}$.

The presence of cosines in the librations because of the dissipative tide has also been pointed out in (Makarov et al. 2016). This study presented a formula very similar to Eq. (92), the amplitudes being denoted as α_s and β_s.

7.3. Numerical validation

Similarly to before, I present numerical simulations of the librations of Epimetheus (Fig. 8) and Mimas (Fig. 9), from the Eq. (80). Here, only phases shifts are depicted, but the validity of the numerical integrations has been also successfully tested on the frequency of the proper oscillations ω_0 and the diurnal amplitude σ_1, which does not significantly differ from the *Amplitude 1* in the Fig. 2 to 7.

The permanent phase lag σ_0 is numerically determined from the constant term in the frequency analysis of the variable $\sigma(t)$ when identified, while the shift in the diurnal libration ϕ_1 should be extracted from the phase of the term oscillating at the frequency $n - \dot{\varpi}$. Unfortunately, I do not have enough accuracy on this phase to get a numerical determination of ϕ_1 with enough confidence, this is why only the analytical result is shown. The plots suggest a good confidence for the expected value of σ_0. I might actually have an error of a few percents.

EDITOR: PLACE FIGURE 8 HERE.

EDITOR: PLACE FIGURE 9 HERE.

No shift has been determined for Epimetheus. The measurements of the librations of Mimas by Tajeddine et al. (2014, Tab. 1) suggest $\phi_1 = (6.35 \pm 0.8)°$, which is too large to be explained with the Maxwell rheology and a Maxwell time of 5 days. This is why I now investigate the influence of the rheology.

8. Influence of the rheology

The Maxwell-Andrade model gives:

$$-\Im(k_2^*) = k_f \frac{A_2 \mathcal{B}}{\mathcal{A}^2 + 2\mathcal{A}A_2 + A_2^2 + \mathcal{B}^2}, \tag{97}$$

the quantitites A_2, $\mathcal{A}$ and $\mathcal{B}$ having already been defined (Eq.59, 65 & 66). As shown in the Fig. 10, this model gives a higher dissipation than the Maxwell model at high frequencies.

EDITOR: PLACE FIGURE 10 HERE.

I here compare the phase shifts given by the Maxwell and Andrade-Maxwell rheologies, for different Maxwell times (Fig. 11 & 12).

EDITOR: PLACE FIGURE 11 HERE.

The phase shifts σ_0 and ϕ_1 have been plotted for Epimetheus for $\alpha = 1.21$, i.e. consistently with the measured libration. We see that the 2 rheological models diverge only for large Maxwell times. The reason for this is that the Andrade-Maxwell rheology considers a high-frequency effect, i.e. the Andrade creep, while the quantities I depict depend on $k_2(\nu_1)$. So, a difference between these 2 models should appear only when the Maxwell time is large with respect to the orbital period. We also see that the phase shifts should be very small, except for Maxwell times that are very short, i.e. a few seconds. This could explain why neither σ_0 nor ϕ_1 has been detected for Epimetheus.

EDITOR: PLACE FIGURE 12 HERE.

As for Epimetheus, the Fig. 12 suggests that the phase shifts should be very small for Mimas. However, Tajeddine et al. (2014) have measured $\phi_1 = 6.35 \pm 0.8°$, which suggests $\tau_M = 27.15^{+4.05}_{-3.15}$ s for a rigidity $\mu = 4$ GPa. A rigidity ten times smaller, i.e. $\mu = 0.4$ GPa,

would give $\tau_M = 270^{+40}_{-31}$ s (Fig. 13). A smaller k_f would give a Maxwell time of the same order of magnitude, since it would be partly counterbalanced by a larger α. For instance, we would have $\alpha = 1.295 \pm 0.033$ and $\tau_M = 18.62^{+2.96}_{-2.23}$ s for a rigidity $\mu = 4$ GPa and $k_f = 1$. These are very small times, if we keep in mind that a Maxwell time of the magnitude of the day is to be expected for ice near its melting point (Nimmo & Manga 2009, e.g.), and larger times for denser materials. Actually, no realistic rigidity results in a realistic Maxwell time.

EDITOR: PLACE FIGURE 13 HERE.

This result discards a model of solid structure for Mimas. In Tajeddine et al. (2014), the authors retained two internal structures which could explain the measured amplitude of libration: a solid body with an excess of triaxiality due to a dense and elongated core, and a global ocean. The phase shift seems to speak for the global ocean.

9. Conclusion

In this study I have proposed a novel theory of librations of a synchronous satellite, in which the role of the frozen component of the inertia of a triaxial satellite is differentiated from the one of the secular elastic deformation. The frozen component should not be addressed as a result of the hydrostatic equilibrium, a recent study by Van Hoolst et al. (2016) mentions this issue. I have shown that the measured physical librations of Epimetheus and Mimas are consistent with the presence of these two components in the inertia of the bodies. However, the introduction of the dissipative tides introduces a phase shift in the librations, which is far too small to explain the one which has been measured for Mimas. This strenghtens the assessment of a global ocean.

The detection of the phase shift in the librations of Mimas is a key result, which should

encourage its investigation for other bodies, because it probably contains information on the ocean. For that, this study should be extended to a more complex structure, in which a solid crust is partly decoupled from a rigid core by a global fluid layer.

Features at the surface of Europa have been interpreted as an evidence for supersynchronous rotation (Geissler et al. 1998), the present study cannot explain it, but an influence of the interior is not to be discarded.

Acknowledgments

This study took benefit from the financial support of the contract Prodex CR90253 from the Belgian Science Policy Office (BELSPO), and is part of the activities of the ISSI Team *Constraining the dynamical timescale and internal processes of the Saturn System from astrometry*. I am indebted to Rose-Marie Baland, Marie Yseboodt, and two anonymous reviewers, for their careful readings and valuable suggestions.

A. Notations used in this paper

EDITOR: PLACE TABLE 6 HERE.

REFERENCES

Cayley A., 1861, Tables of the developments of functions in the theory of elliptic motion, Memoirs of the Royal Astronomical Society, 29, 191-306

Charnoz S., Crida A., Castillo-Rogez J.C., Lainey V., Dones L., Karatekin Ö., Tobie G., Mathis S., Le Poncin-Lafitte C. & Salmon J., 2011, Accretion of Saturn's mid-sized moons during the viscous spreading of young massive rings: Solving the paradox of silicate-poor rings versus silicate-rich moons, Icarus, 216, 535-550

Correia A.C.M. & Rodríguez A., 2013, On the equilibrium figure of close-in planets and satellites, ApJ, 767:128

Duriez L., Cours de mécanique céleste, `http://lal.univ-lille1.fr/mecanique_celeste.html`, in French

Efroimsky M., 2012a, Bodily tides near spin-orbit resonances, Celestial Mechanics and Dynamical Astronomy, 112, 283-330

Efroimsky M., 2012b, Justification of the two-bulge method in the theory of bodily tides, A&A, 544, A133

Garrick-Bethell I., Perera V., Nimmo F. & Zuber M.T., 2014, The tidal-rotational shape of the Moon and evidence for polar wander, Nature, 512, 181-184

Geissler P.E., Greenberg R., Hoppa G., Helfenstein P., McEwen A., Pappalardo R., Tufts R., Ockert-Bell M., Sullivan R., Greeley R., Belton M.J.S., Denk T., Clark B., Burns J., Veverka J. & the Galileo Imaging Team, 1998, Evidence for non-synchronous rotation of Europa, Nature, 391, 368-370

Goldreich P. & Sari R., 2009, Tidal evolution of rubble piles, ApJ, 691, 54-60

Goldreich P.M. & Mitchell J.L., 2010, Elastic ice shells of synchronous moons: Implications for cracks on Europa and non-synchronous rotation of Titan, Icarus, 209, 631-638

Henrard J., 2005, The rotation of Io, Icarus, 178, 144-153

Iess L., Rappaport N.J., Jacobson R.A., Racioppa P., Stevenson D.J., Tortora P., Armstrong J.W. & Asmar S.W., 2010, Gravity field, shape, and moment of inertia of Titan, Science, 327, 1367-1369

Iess L., Stevenson D.J., Parisi M., Hemingway D., Jacobson R.A., Lunine J.I., Nimmo F., Armstrong J.W., Asmar S.W., Ducci M. & Tortora P., 2014, The gravity field and interior structure of Enceladus, Science, 344, 78-80

Jacobson R.A., Antreasian P.G., Bordi J.J., Criddle K.E., Ionasescu R., Jones J.B., Mackenzie R.A., Meek M.C., Parcher D., Pelletier F.J., Owen Jr. W.M., Roth D.C., Roundhill I.M. & Stauch J.R., 2006, The gravity field of the Saturnian System from satellite observations and spacecraft tracking data, AJ, 132, 2520-2526

Jacobson R.A., Spitale J., Porco C.C., Beurle K., Cooper N.J., Evans M.W. & Murray C.D., 2008, Revised orbits of Saturn's small inner satellites, AJ, 135, 261-263

Jeffreys H., 1937, On the figures of the Earth and Moon, Geophysical Journal International, 4, 1-13

Karato S.-I., 2008, Deformation of Earth materials – An introduction to the rheology of solid Earth, Cambridge University Press, Cambridge

Kaula W.M., 1966, Theory of satellite geodesy, Blaisdell Publishing Company, Waltham, MA

Lambeck K. & Pullan S., 1980, The lunar fossil bulge hypothesis revisited, Physics of the Earth and Planetary Interiors, 22, 29-35

Laskar J., 1999, Introduction to frequency analysis. In: Proceedings of 3DHAM95 NATO Advanced Institute, S'Agaro, 553, 134-150

Laskar J., 2005, Frequency map analysis and quasiperiodic decompositions. In: Benest et al. (Eds.), Hamiltonian systems and Fourier analysis: New prospects for gravitational dynamics, Cambridge scientific publishers, 99-129

Le Maistre S., Rosenblatt P., Rambaux N., Castillo-Rogez J.C., Dehant V. & Marty J.-C., 2013, Phobos interior from librations determination using Doppler and star tracker measurements, Planet. Space Sci., 85, 106-122

Makarov V.V., Frouard J. & Dorland B., 2016, Forced libration of tidally synchronized planets and moons, MNRAS, 456, 665-671

Matsuyama I. & Nimmo F., 2009, Gravity and tectonic patterns of Mercury: Effect of tidal deformation, spin-orbit resonance, nonzero eccentricity, despinning, and reorientation, J. Geophys. Res., 114, E01010

Meriggiola R., Iess L., Stiles B.W., Lunine J.I. & Mitri G., 2016, The rotational dynamics of Titan from Cassini RADAR images, Icarus, 275, 183-192

Meyer J. & Wisdom J., 2008, Tidal evolution of Mimas, Enceladus, and Dione, Icarus, 193, 213-223

Murray C.D. & Dermott S.F., 2000, Solar System Dynamics, Cambridge University Press, Cambridge

Nimmo F. & Manga M., 2009, Geodynamics of Europa's icy shell, in: Europa, Pappalardo R.T., McKinnon W.B. & Khurana K. eds., The University of Arizona Press, Tucson

Noyelles B., Lemaître A. & Vienne A., 2008, Titan's rotation: A 3-dimensional theory, A&A, 478, 959-970

Noyelles B., 2010, Theory of the rotation of Janus and Epimetheus, Icarus, 207, 887-902

Noyelles B., Karatekin Ö. & Rambaux N., 2011, The rotation of Mimas, A&A, 536, A61

Richard A., Rambaux N. & Charnay B., 2014, Librational response of a deformed 3-layer Titan perturbed by non-Keplerian orbit and atmospheric couplings, Planet. Space Sci., 93-94, 22-34

Richard A., 2014, Modèle de satellite à trois couches élastiques : application à la libration en longitude de Titan et Mimas, PhD dissertation, Paris Observatory, in French

Robutel P., Rambaux N. & Castillo-Rogez J., 2011, Analytical description of physical librations of saturnian coorbital satellites Janus and Epimetheus, Icarus, 211, 758-769

Stiles B.W., Kirk R.L., Lorenz R.D., Hensley S., Lee E., Ostro S.J., Allison M.D., Callahan P.S., Gim Y., Iess L., Persi Del Marmo P., Hamilton G., Johnson W.T.K. & West R.D., 2008, Determining Titan's spin state from CASSINI RADAR images, AJ, 135, 1669-1680

Tajeddine R., Rambaux N., Lainey V., Charnoz S., Richard A., Rivoldini A. & Noyelles B., 2014, Constraints on Mimas' interior from Cassini ISS libration measurements, Science, 346, 322-324

Thomas P.C., 2010, Sizes, shapes, and derived properties of the saturnian satellites after the Cassini nominal mission, Icarus, 208, 395-401

Thomas P.C., Tajeddine R., Tiscareno M.S., Burns J.A., Joseph J., Loredo T.J., Helfenstein P. & Porco C., 2016, Enceladus's measured physical libration requires a global subsurface ocean, Icarus, 264, 37-47

Tiscareno M.S., Thomas P.C. & Burns J.A., 2009, The rotation of Janus and Epimetheus, Icarus, 204, 254-261

Tortora P., Zannoni M., Hemingway D., Nimmo F., Jacobson R.A., Iess L. & Parisi M., 2016, Rhea gravity field and interior modeling from Cassini data analysis, Icarus, 264, 264-273

Tricarico P., 2014, Multi-layer hydrostatic equilibrium of planets and synchronous moons: Theory and application to Ceres and to Solar system moons, ApJ, 782:99

Van Hoolst T., Baland R.-M. & Trinh A., 2013, On the librations and tides of large icy satellites, Icarus, 226, 299-315

Van Hoolst T., Baland R.-M. & Trinh A., 2016, The diurnal libration and interior structure of Enceladus, Icarus, 277, 311-318

Vienne A. & Duriez L., 1995, TASS1.6: Ephemerides of the major Saturnian satellites, A&A, 297, 588-605

Williams J.G., Boggs D.H., Yoder C.F., Ratcliff J.T. & Dickey J.O., 2001, Lunar rotational dissipation in solid body and molten core, J. Geophys. Res., 106, 27933-27968

Williams J.G. & Boggs D.H., 2015, Tides on the Moon: Theory and determination of dissipation, Journal of Geophysical Research: Planets, 120, 689-724

Zahn J.-P., 1966, Les marées dans une étoile double serrée, Annales d'Astrophysique, 29, 313-330, in French

Zebker H.A., Stiles B., Hensley S., Lorenz R., Kirk R.L. & Lunine J., 2009, Size and shape of Saturn's moon Titan, Science, 324, 921-923

This manuscript was prepared with the AAS LaTeX macros v5.2.

List of Tables

1 Orbital dynamics and gravity field of the main satellites of Saturn 38

2 Shapes of the main satellites of Saturn 39

3 Departures from the hydrostatic equilibrium 39

4 Comparison with previous studies 40

5 Physical and dynamical parameters used for Epimetheus and Mimas 40

6 Main notations used in this study. 41

Table 1: Orbital dynamics and gravity field of the main satellites of Saturn. The orbital data are mean Keplerian elements given by the JPL HORIZON portal, except for the eccentricity of Enceladus that is taken from (Vienne & Duriez 1995), and the mean motions of Janus and Epimetheus, taken from (Noyelles 2010). The masses come from (Jacobson et al. 2006, 2008), and the Stokes coefficients from (Iess et al. 2014; Tortora et al. 2016; Iess et al. 2010). Two gravity solutions have been published for Rhea and Titan.

Satellites	$\mathcal{G}M$	n	e	J_2	C_{22}
	($\mathrm{km}^3.\mathrm{s}^{-2}$)	(rad/y)	($\times 100$)	($\times 10^5$)	($\times 10^5$)
Janus	0.12660	3304.014328	0.68	–	–
Epimetheus	0.03513	3304.014328	0.98	–	–
Mimas	2.5023	2435.144271	1.96	–	–
Enceladus	7.2096	1674.867267	0.5	543.25	154.98
Tethys	41.2097	1215.663921	0.01	–	–
Dione	73.1127	838.510861	0.22	–	–
Rhea (SOL 1)	153.9416	508.009307	0.02	94.60	24.21
(SOL 2)				95.70	22.70
Titan (SOL 1)	8978.1356	143.924045	2.88	3.1808	0.9983
(SOL 2)				3.3462	1.0022

Table 2: Shapes of the main satellites of Saturn

Satellites	$\mathfrak{a} \times \mathfrak{b} \times \mathfrak{c}$ (km× km× km)	R (km)	References	q ($\times 10^3$)
Janus	$101.5 \times 92.5 \times 76.3$	89.5	Tiscareno et al. (2009)	62.07
Epimetheus	$64.9 \times 57.0 \times 53.1$	58.1	Tiscareno et al. (2009)	61.20
Mimas	$206.60 \times 195.73 \times 190.47$	197.49	Tajeddine et al. (2014)	18.33
Enceladus	$256.2 \times 251.4 \times 248.6$	252.24	Thomas et al. (2016)	6.270
Tethys	$538.4 \times 528.3 \times 526.3$	531.0	Thomas (2010)	5.391
Dione	$563.4 \times 561.3 \times 559.6$	561.4	Thomas (2010)	1.709
Rhea	$765.0 \times 763.1 \times 762.4$	736.5	Thomas (2010)	0.749
Titan	$2575.15 \times 2574.78 \times 2574.47$	2574.73	Zebker et al. (2009)	0.040

Table 3: Departures from the hydrostatic equilibrium. The theoretical numbers come from the Eq.(4) and (5).

Satellites	$(\mathfrak{b}-\mathfrak{c})/(\mathfrak{a}-\mathfrak{c})$			J_2/C_{22}		
	Measured	Theoretical	Error	Measured	Theoretical	Error
Janus	0.643	0.113	469.4%	–	2.151	–
Epimetheus	0.331	0.115	187.6%	–	2.169	–
Mimas	0.326	0.210	55.2%	–	2.989	–
Enceladus	0.368	0.236	56.0%	3.505	3.214	9.1%
Tethys	0.165	0.238	30.6%	–	3.231	–
Dione	0.447	0.246	81.7%	–	3.301	–
Rhea (SOL 1)	0.269	0.248	8.4%	3.907	3.319	17.7%
(SOL 2)				4.216		27.0%
Titan (SOL 1)	0.456	0.251	81.5%	3.186	3.342	4.7%
(SOL 2)				3.339		0.09%

Table 4: Comparison with previous studies. The formulae labeled *This study* are given by the Eq. 49 and 50, but there expansion is here limited to the degree 1 in the eccentricity.

	Van Hoolst et al. (2013)	Richard et al. (2014)	This study
ω_0^2	$3n^2\frac{B-A}{C}\left(1-\frac{k_2}{k_f}\right)$	$3n^2\frac{B-A}{C}$	$3n^2\frac{(I_{22}-I_{11})^{(f)}}{\frac{2}{5}MR^2+\frac{5}{9}k_f M_{\eta}\frac{R^5}{a^3}}$
κ_1	$6en^2\frac{B-A}{C}\left(1-\frac{5}{6}\frac{k_2}{k_f}\right)$	$6en^2\left(\frac{B-A}{C}-\frac{h_2}{2}M_{\eta}\frac{R^5}{Ca^3}\right)$	$6en^2\frac{(I_{22}-I_{11})^{(f)}+M_{\eta}\frac{R^5}{a^3}\left(k_f-k_2(\nu_1)\right)}{\frac{2}{5}MR^2+\frac{5}{9}k_f M_{\eta}\frac{R^5}{a^3}}$

Table 5: Physical and dynamical parameters used for Epimetheus and Mimas. The densities ρ and the dynamical parameters n, a, e and $\dot{\varpi}$ come from JPL HORIZONS, except for the eccentricity of Epimetheus that is the one recommended by Tiscareno et al. (2009). The rigidity μ of Epimetheus is the one used by Robutel et al. (2011), itself derived from (Goldreich & Sari 2009) in assuming Epimetheus to be a rubble-pile, while the one of Mimas is taken from (Meyer & Wisdom 2008). The Love numbers are computed from the Maxwell model (Eq. 61).

	Epimetheus	Mimas
μ	2×10^8 Pa	4×10^9 Pa
τ_M	5 d	5 d
ρ	6.4×10^2 kg/m^3	1.15×10^3 kg/m^3
g	1.04×10^{-2} m/s^2	6.365×10^{-2} m/s^2
A_2	4.914×10^3	2.618×10^3
$k_2(\nu_1)/k_f$	2.035×10^{-4}	3.818×10^{-4}
n	9.0425 rad/d	6.66706 rad/d
$\dot{\varpi}$	3.6×10^{-2} rad/d	1.745×10^{-2} rad/d
e	9.8×10^{-3}	1.96×10^{-2}
a	151 453 km	185 565 km

Table 6. Main notations used in this study.

$\mathfrak{a}$, $\mathfrak{b}$, $\mathfrak{c}$, R	External radii and mean radius of the satellite
n, a, e	Mean motion, semimajor axis and eccentricity of the satellite
λ, f, $\mathcal{M}$	Mean longitude, true longitude and mean anomaly of the satellite
ϖ, $\dot{\varpi}$	Longitude of the pericenter of the satellite, and its precessional rate
J_2, C_{22}	Stokes coefficients of the satellite
$M_{\mathfrak{h}}$, M	Masses of the parent planet (here Saturn) and the satellite
ρ, g	Density and surface gravity of the satellite
X, Y, Z	Cartesian coordinates of a mass element of the satellite
$\mathfrak{r}$, θ, ℓ	Spherical coordinates of a mass element of the satellite
$x = x_1$, $y = x_2$, $z = x_3$	Cartesian coordinates of the unit vector pointing to the planet
$\mathcal{I}^{(f)}$, $\mathcal{I}^{(e)}$, $\mathcal{I}$	Frozen, elastic, and global tensors of inertia
$\mathcal{I}^{(r)}$, $\mathcal{I}^{(t)}$, $\mathcal{I}^{(v)}$	Rotational, tidal, and viscoelastic tensors of inertia
I_{ij}	Components of the tensor of inertia
τ_M, τ_A	Maxwell and Andrade times
p, $\sigma = p - \lambda + \pi$	Rotation angle and argument of the synchronous resonance
N	Andrade parameter
μ, η	Rigidity and viscosity

List of Figures

1 Elastic tides 43

2 Rotational quantities for Epimetheus, in considering an excess of triaxiality . 43

3 Excess of triaxiality for Epimetheus, for different k_f. 44

4 Rotational quantities for Epimetheus, for $C_{22} = 1.426 \times 10^{-2}$ 44

5 Rotational quantities for Mimas, with an excess of triaxiality 45

6 Excess of triaxiality for Mimas, for different k_f. 45

7 Rotational quantities for Mimas, for $C_{22} = 5.606 \times 10^{-3}$ 46

8 Rotational quantities for Epimetheus in the dissipative case 47

9 Rotational quantities for Mimas in the dissipative case 48

10 Dissipative tides 49

11 Influence of the rheology on the rotation of Epimetheus 49

12 Influence of the rheology on the rotation of Mimas 50

13 Deduced Maxwell times for Mimas 50

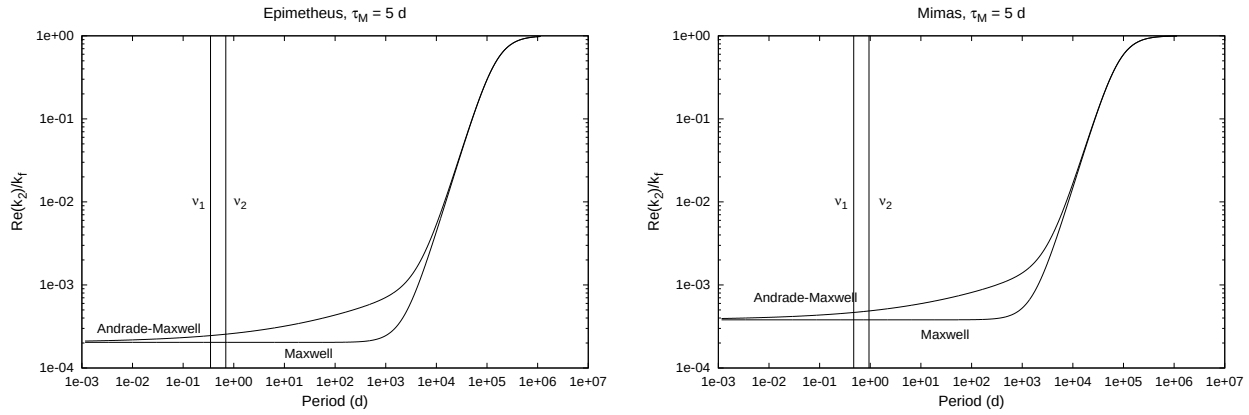

Fig. 1.— Elastic tides for Epimetheus and Mimas. The Andrade time is set equal to the Maxwell time, and the Andrade parameter N to 0.3. The two vertical lines represent the diurnal and semi-diurnal periods. We can see that there are few differences between the two models.

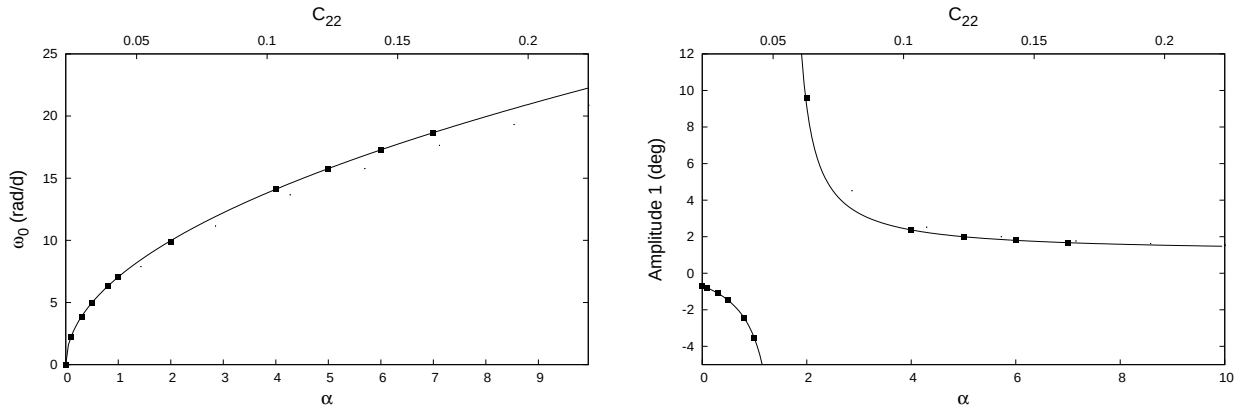

Fig. 2.— Rotational quantities for Epimetheus, in considering an excess of triaxiality, for $k_f = 1.5$. The lines come from the analytical formulae (67, 49 & 51), while the squares are the results from numerical simulations. The *Amplitude 1* is the amplitude of response at the diurnal frequency $n - \dot{\varpi}$.

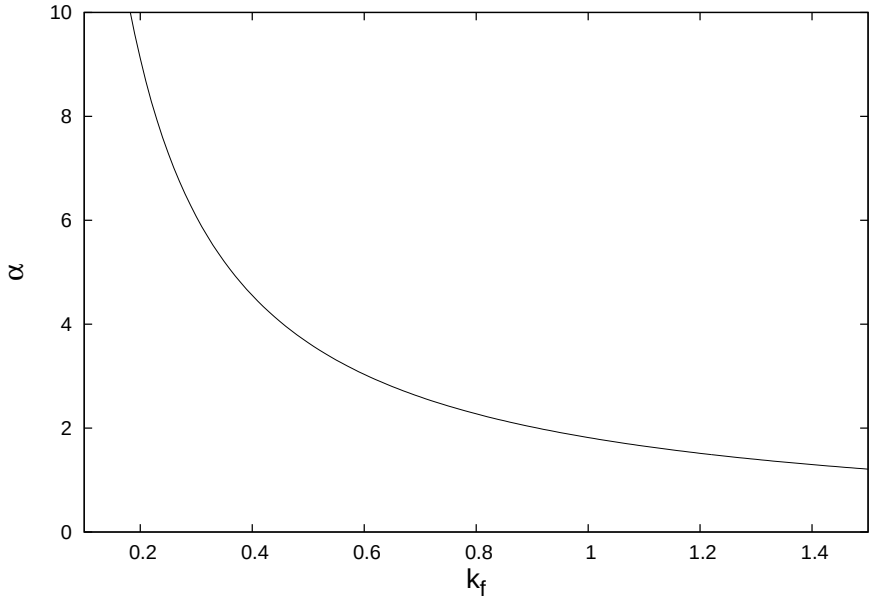

Fig. 3.— Excess of triaxiality for Epimetheus, for different k_f.

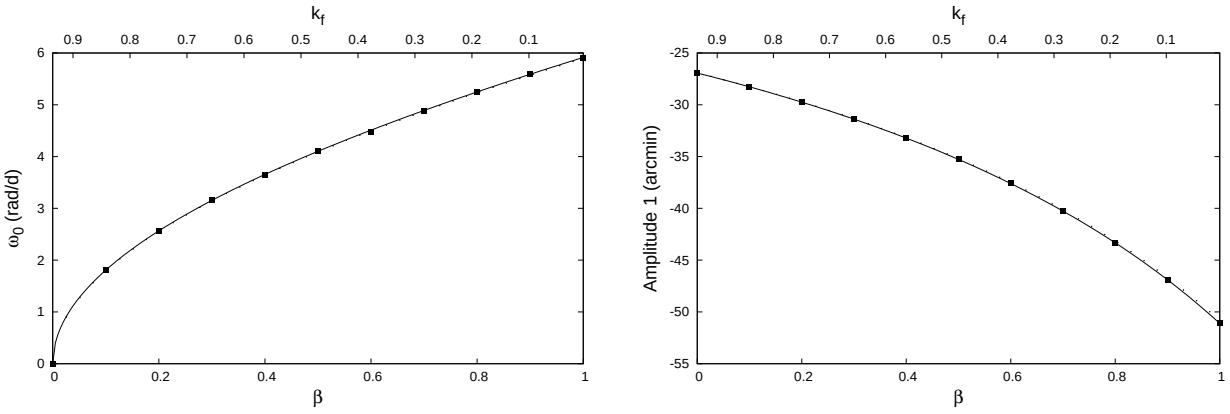

Fig. 4.— Rotational quantities for Epimetheus, for $C_{22} = 1.426 \times 10^{-2}$, as suggested by the measured shape. The lines come from the analytical formulae, while the squares are the results of numerical simulations.

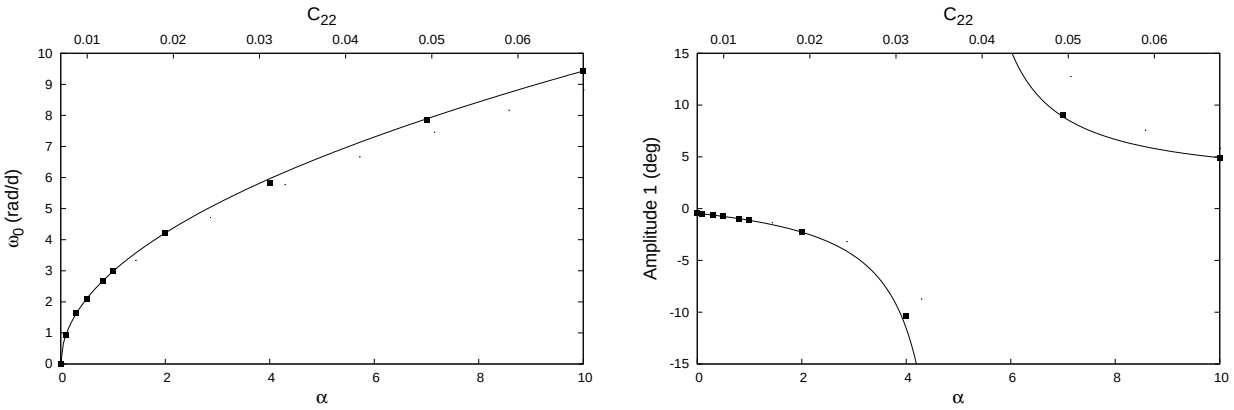

Fig. 5.— Rotational quantities for Mimas, with an excess of triaxiality, for $k_f = 1.5$.

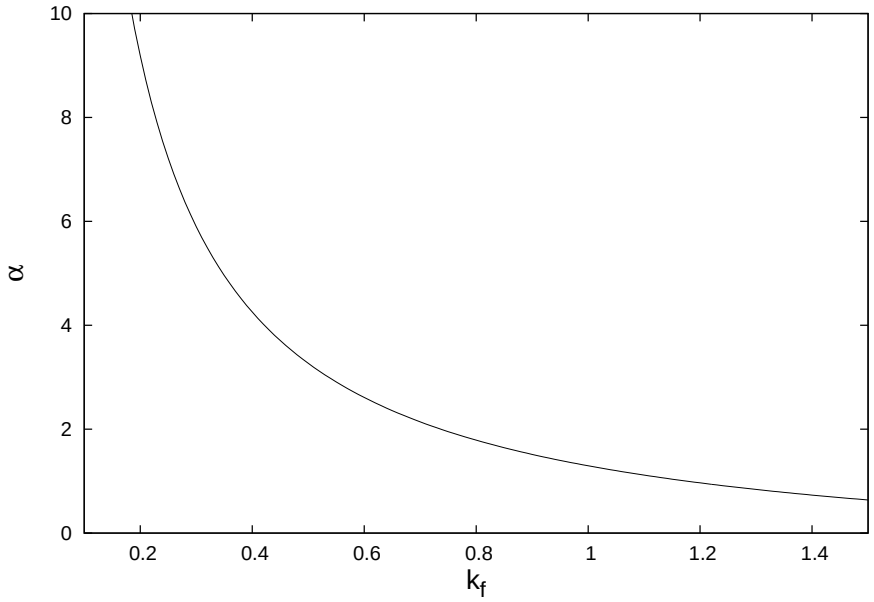

Fig. 6.— Excess of triaxiality for Mimas, for different k_f.

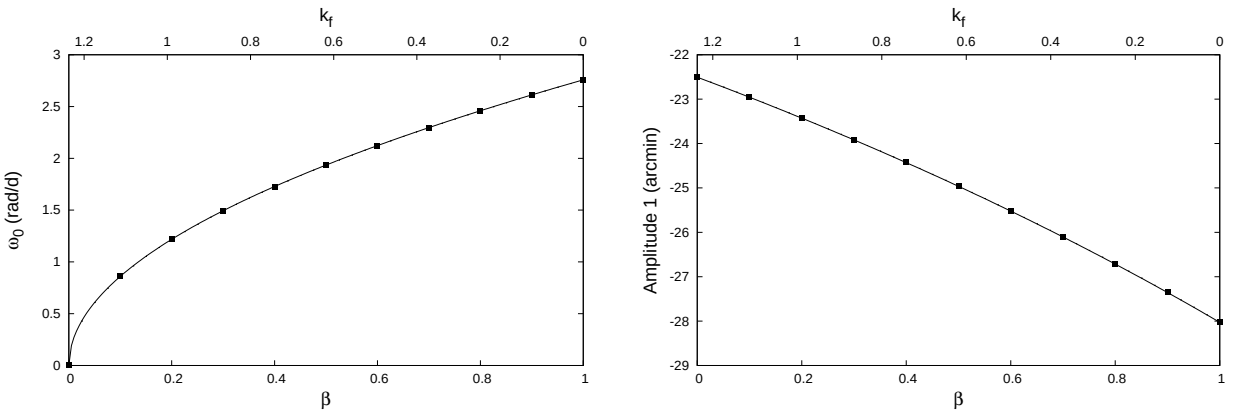

Fig. 7.— Rotational quantities for Mimas, for $C_{22} = 5.606 \times 10^{-3}$, deduced from the measured shape.

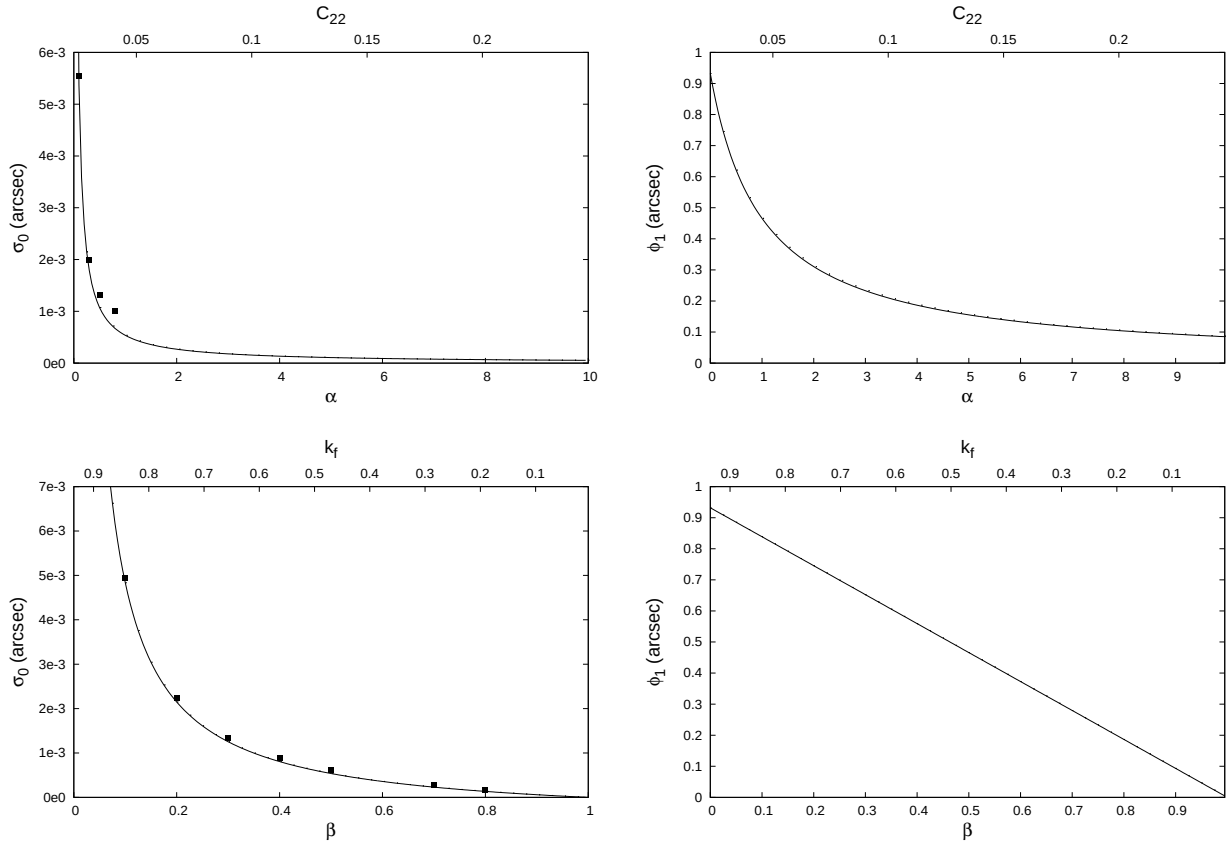

Fig. 8.— Rotational quantities for Epimetheus in the dissipative case, for $k_f = 1.5$ (top), and $C_{22} = 1.426 \times 10^{-2}$ (down). The lines come from the analytical formulae, while the squares result from numerical simulations.

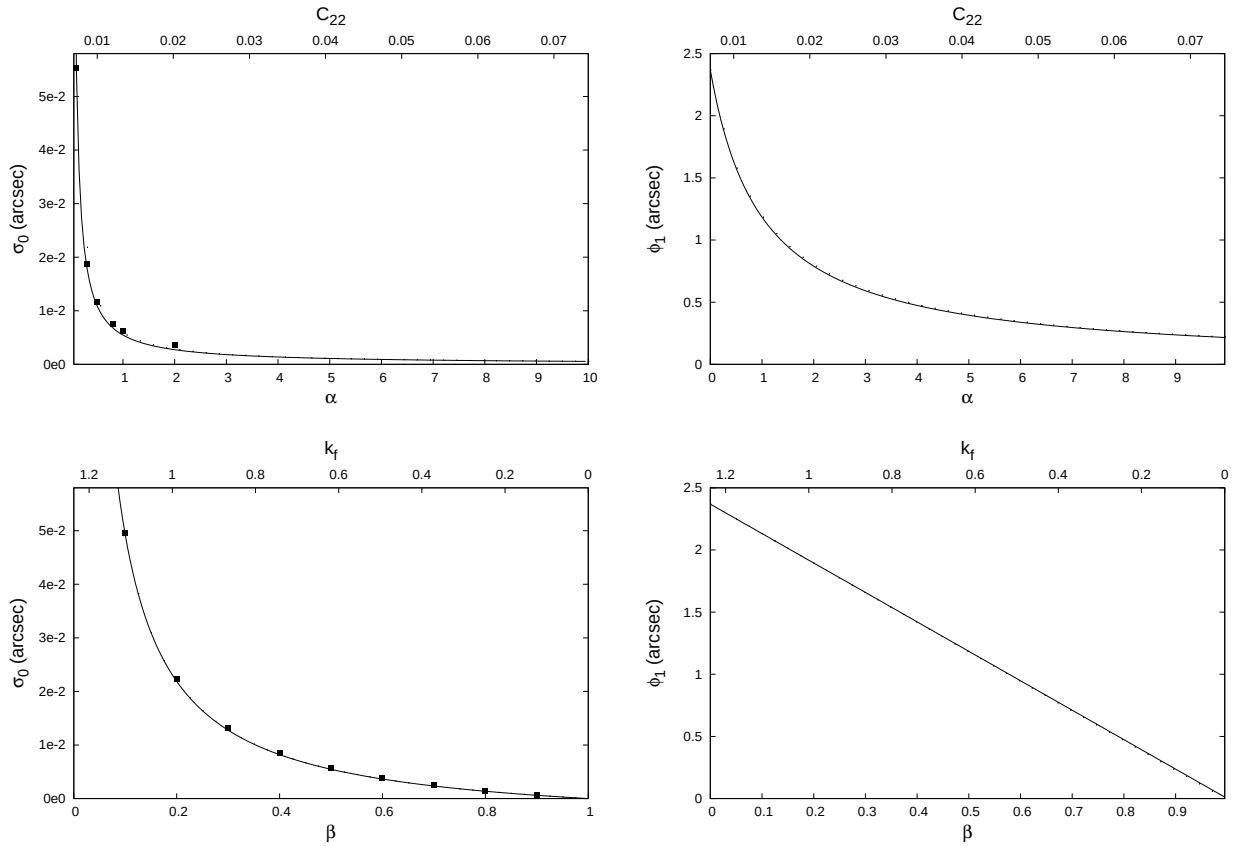

Fig. 9.— Rotational quantities for Mimas in the dissipative case, for $k_f = 1.5$ (top), and $C_{22} = 5.606 \times 10^{-3}$ (down). The lines come from the analytical formulae, while the squares result from numerical simulations.

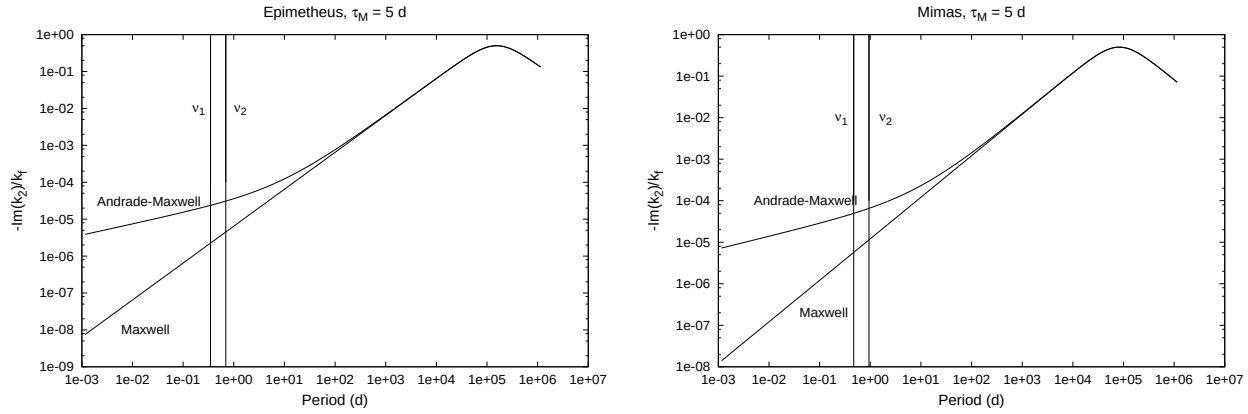

Fig. 10.— Dissipative part of the tides, for the Maxwell and Andrade-Maxwell models. We can see a significant discrepancy for high-frequency excitations, which affects the quantity k_2/Q at the diurnal and semi-diurnal frequencies.

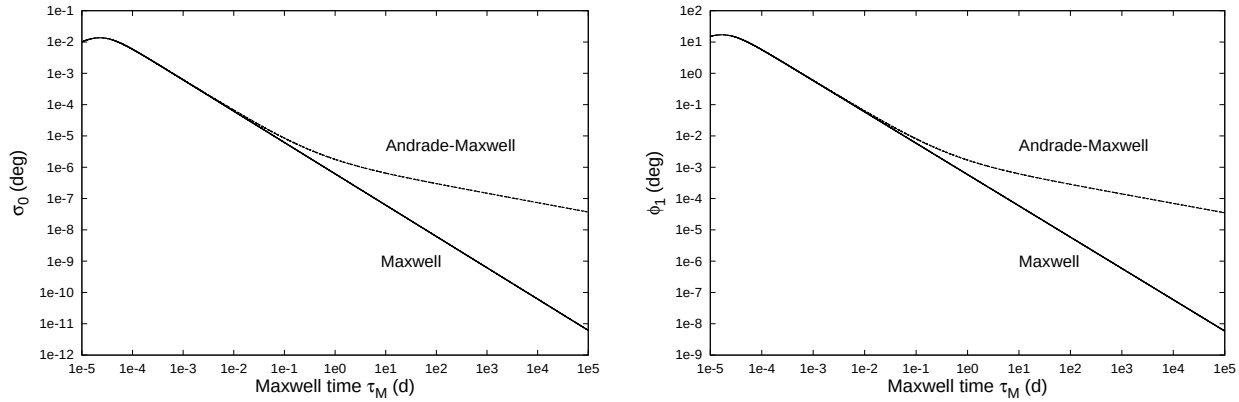

Fig. 11.— Influence of the rheology on the rotation of Epimetheus, for $\alpha = 1.21$. The Andrade-Maxwell model has been applied with $N = 0.3$, this parameter influencing the slope for high Maxwell times.

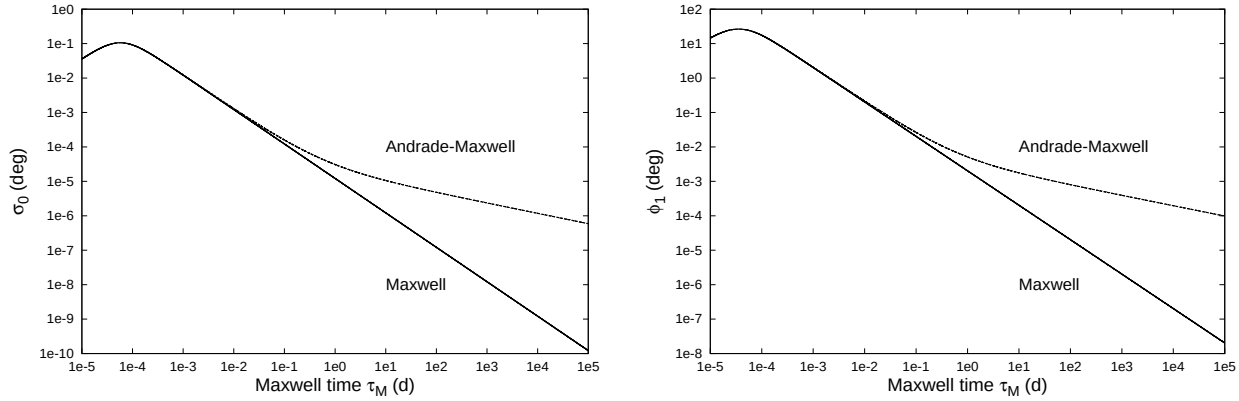

Fig. 12.— Influence of the rheology on the rotation of Mimas, for $\alpha = 0.6225$, and $N = 0.3$.

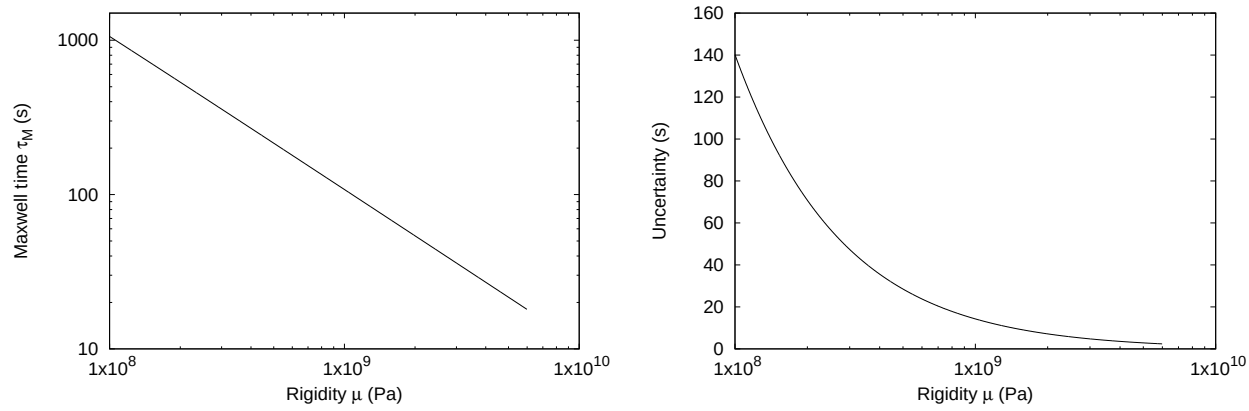

Fig. 13.— Maxwell times of Mimas deduced from the diurnal phase shift ϕ_1 (left), and the uncertainty associated (right). These numbers are much shorter than expected from our knowledge of Mimas.